International Journal of Nanomedicine

Dovepress
Taylor & Francis Group

Open Access Full Text Article

ORIGINAL RESEARCH

Dual-Responsive Methotrexate-Human Serum Albumin Complex-Encapsulated Liposomes for Targeted and Enhanced Atherosclerosis Therapy

Xueqin Wang[1,*], Xiaodong Chen[1,*], Huawen Ji[1,*], Along Han[2], Chengxi Wu[1], Jun Jiang[1], Yu Nie[3], Chunhong Li[4], Xiangyu Zhou[1]

[1]Department of Thyroid Surgery, Affiliated Hospital, Southwest Medical University, Luzhou, People's Republic of China; [2]Beijing Advanced Innovation Center for Soft Matter Science and Engineering, State Key Laboratory of Organic–Inorganic Composites, State Key Laboratory of Chemical Resource Engineering, Beijing Laboratory of Biomedical Materials, Bionanomaterials & Translational Engineering Laboratory, Beijing Key Laboratory of Bioprocess, Beijing University of Chemical Technology, Beijing, People's Republic of China; [3]National Engineering Research Center for Biomaterials, Sichuan University, Chengdu, People's Republic of China; [4]Department of Pharmaceutical Sciences, School of Pharmacy, Southwest Medical University, Luzhou, People's Republic of China

*These authors contributed equally to this work

Correspondence: Chunhong Li, Email lispringhong@126.com; Xiangyu Zhou, Email xiangyuzhou971@vip.126.com

Introduction: In plaque sites of atherosclerosis (AS), the physiological barrier caused by the thick fiber cap due to the overmigration of vascular smooth muscle cells (VSMCs) prevents efficient drug delivery to damaged macrophages. How to ensure precise targeted delivery of drugs to plaque sites and their on-demand release to dysfunctional cells under the thick fibrous cap are feasible solutions to enhance AS treatment.

Methods: A small complex of methotrexate (MTX)-human serum albumin (HSA) with strong, thick fibrous cap penetration ability was encapsulated in a cholesterol hemisuccinate (CHEM) prepared pH-sensitive liposome, modifying with ROS-responsive PEG2000-TK-DSPE (PTD), termed PTD/Lipo/MTX-HSA.

Results: PTD/Lipo/MTX-HSA can achieve precise targeting and on-demand release in response to plaques environments of AS. The designed formulation accelerated the release of the small-sized MTX-HSA complex in response to excess ROS and acidic pH conditions, and it better penetrated the macrophage spheroids. Furthermore, it has precise targeting ability in the AS mouse model and can produce good anti-inflammatory efficacy by inhibiting p65 entry into the nucleus turn out inflammatory factor.

Conclusion: Our formulations work with safety in mind, and it also highlights the potential of precisely targeted and on-demand-released dual-responsive smart nanoplatforms as promising therapeutic options to penetrate deeper plaques for the effective treatment of AS.

Keywords: methotrexate-human serum albumin complex, dual-responsive smart liposomes, penetration of deeper plaques

Introduction

The incidence of atherosclerosis (AS), a chronic inflammatory disease, is increasing globally as the population ages.[1,2] Endothelial injury is considered the initiating factor of atherosclerosis,[3] which leads to endothelial dysfunction, allowing easy penetration of lipids from the blood into the vessel wall. Subsequently, macrophages and vascular smooth muscle cells (VSMCs) phagocytose lipids, forming foam cells and releasing proinflammatory factors that trigger a local inflammatory response. Recent research has shown that AS is a VSMC-driven tumor-like disease, and the proliferation and migration of VSMCs leads to the formation of a thick fibrous cap, hindering effective therapeutic drug delivery to damaged macrophages in plaques. Therefore, it holds great promise for overcoming physiological barriers to delivering drugs to damaged macrophages to enhance AS treatment.[4,5] Most of the research on nanoparticle drug delivery has focused on larger particles, which have long circulation periods; however, their permeability is poor because only

Received: 13 November 2024
Accepted: 5 February 2025
Published: 21 February 2025

nanoparticles less than 40 nm in size can penetrate thick fiber caps.[6] Therefore, the design of precise targeted drug delivery systems with size-adjustable formulations, which have long circulation times in blood, and the on-demand release of small nanoparticles to reach dysfunctional cells in deeper plaques in response to inflammatory stimuli constitute an attractive therapeutic strategy for AS.

Excess reactive oxygen species (ROS) are produced by pathologic resident cells in the local microenvironment.[7–9] In addition, the rapid proliferation of inflammatory cells results in increased levels of aerobic glycolysis and lactic acid, resulting in an acidic environment at plaque sites.[10,11] An increase in ROS and a low pH are the typical features of plaque sites that distinguish blood vessels from normal tissues.[12] These specific pathological milieus provide potential targets for the design of on-demand dual-responsive drug delivery systems for AS treatment.

Recently, single pH- or ROS-responsive drug delivery systems have achieved favorable anti-inflammatory effects in AS treatment; however, some challenges still need to be solved. First, multistep synthetic procedures involving pH- or ROS-responsive nanoplatforms result in low reproducibility and increase the risk of introducing harmful impurities.[13] Second, a single-responsive drug delivery system might face the challenge of inadequate responsiveness, further leading to deficient on-demand drug release.[13] Compared with single-responsive nanoparticles, dual-responsive nanoplatforms might have more sensitive responsiveness to the local inflammatory environment, which is beneficial for achieving on-demand drug release. To this end, we aimed to develop a facile method to prepare a dual-stimuli-responsive size-adjustable drug delivery system with simpler preparation procedures, which could increase the reproducibility and potential for clinical translation.

In our previous study, we constructed a pH-sensitive liposome encapsulating a small-sized methotrexate (MTX)-human serum albumin (HSA) complex, namely, Lipo/MTX-HSA, which could achieve variable particle sizes in response to low pH conditions.[14] However, this naked single-responsive size-adjustable liposome drug delivery system may face the challenges of premature drug release, low targeting efficiency, and deficient controlled release, which might result in low penetration into deeper plaques and poor therapeutic effects.

In the present study, an ROS-sensitive linker called a thioketal (TK)-based polymer (PEG2000-TK-DSPE, PTD) was introduced to modify the outer liposome membrane of Lipo/MTX-HSA to prepare the ROS and pH-sensitive nanoplatform PTD/Lipo/MTX-HSA, with the aim of enabling precise delivery to the targeted area. At high ROS levels in the plaque microenvironment, the TK bond of PTD is destroyed, and further liposomes are degraded in response to local low pH conditions. Then, small MTX-HSA complexes are released, resulting in the release of "smarter" controlled drugs and effective penetration of the plaque to reach dysfunctional cells, enhancing the therapeutic effect by inhibiting p65 entry into the nucleus. Our study provides a novel therapeutic strategy for precise targeting to plaque sites and on-demand release of small complexes that easily cross the physiological barrier to dysfunctional cells for effective treatment of AS, suggesting great potential for clinical translation.

Materials and Methods

Cells and Animals

Human umbilical vein endothelial cells (HUVECs), human aortic smooth muscle cells (HASMCs) and Raw264.7 cells were purchased from CTCC (cat: CTCC-0804-PC; cat: CTCC-001-0577; cat: SCSP-5036). The cells were treated with LPS (Solarbio, cat: IL2020) to establish an in vitro model of chronic inflammation and with oxidized low-density lipoprotein (ox-LDL, Yiyuanbiotech, cat: YB002) to establish an in vitro model of lipid oxidation.

Male ApoE$^{-/-}$ mice (18±2 g) were obtained from Chengdu Pharmachem and maintained under standard specific pathogen-free (SPF) conditions at the Animal Experiment Centre of Southwest Medical University. The specific modeling method involved feeding 8-week-old mice a high-fat diet (Research Diets; cat: D12108C) until 20 weeks of age and then tail vein injections of saline, MTX, MTX-HSA, Lipo/MTX-HSA or PTD/Lipo/MTX-HSA (n=6) every 3 days 8 times. Samples were taken two days after the last injection. The surgical methods and experimental protocols were approved by the Animal Experimentation Committee of Southwest Medical University (approval number swmu20220112) prior to performing animal experiments. Approval for all animal experiments was obtained from the Animal Care and Ethics Committee of Southwest Medical University (license no. 20231020–016). All animal

experimental procedures were performed in accordance with the requirements of the National Research Council's Guide for the Care and Use of Laboratory Animals.

Preparation of a Small-Sized MTX-HSA Complex and Its Ability to Penetrate Raw264.7 Cell Spheroids

MTX-HSA with a small particle size was first prepared by dissolving MTX ($C_{20}H_{20}N_8Na_2O_5$ source leaf, cat: S26260) at 2 mg/mL in methanol; HSA was subsequently dissolved at 4 mg/mL in PBS. MTX:HSA was then mixed at 2:1, 4:1, and 40:1 mole ratios (Table 1) and lightly stirred for 3 h. Next, the MTX-HSA complex was collected by centrifugation at 6000 rpm for 30 min in a 10 kDa ultrafiltration tube for lyophilization. For the preparation of fluorescent nanoparticles, MTX was replaced with DID (Beyotime Biotechnology, cat: C1039). The spheroids were prepared with Raw264.7 cells via the hanging drop/agarose method.[15] The macrophage spheroids were incubated with different sizes of DID-HSA to study their penetration ability and investigate the most favorable size.

Preparation of PTD/Lipo/MTX-HSA

We prepared size-tunable nanoparticles (PTD/Lipo/MTX-HSA) via ethanol injection. CHEMS ($C_{27}H_{46}O$, KESHI), PEG2000-TK-DSPE (Xi'an Ruixi Biological Technology Co., Ltd., cat: R-D526-2K) and egg yolk lecithin E80 (Beijing Solarbio Science & Technology Co., Ltd., cat: L8260) were dissolved in ethanol at a mass ratio of 1:1:4 as the oil phase, and the MTX-HSA complex was dissolved in PBS as the water phase. The oil phase was injected into the water phase at a rate of 0.5 mL/min (while stirring), stirred slowly for 2 h at 40°C in a water bath, and then filtered through a 0.22 μm microporous membrane.

Characterization of PTD/Lipo/MTX-HSA

The hydrodynamic diameters and zeta potentials were examined via a Malvern Zetasizer Nano ZS90 (Malvern Ltd., UK). The morphology of the NPs was observed via transmission electron microscopy (TEM, JEM 100CX, JEOL Co. Ltd., Tokyo, Japan). The freeze-dried samples were scanned via a Fourier transform infrared spectrometer (FT-IR, Nicolet 6700, USA) with a scanning range of 4000–400 cm^{-1}. In addition, the encapsulation efficiency (EE) and drug loading efficiency (DLE) of MTX were measured via high-performance liquid chromatography (HPLC, LC-2030, Japan). M1 represents free MTX, M_2 represents total MTX, and M_3 represents the total mass of the preparation.

$$EE(\%)=(M_2-M_1)/M_2\times 100\%$$

$$DLE(\%)=(M_2-M_1)/M_3\times 100\%$$

In vitro Stability and Release Kinetics of PTD/Lipo/MTX-HSA

The MTX release efficiency of PTD/Lipo/MTX-HSA was investigated. Briefly, 1 mL of PTD/Lipo/MTX-HSA (1 mg/mL MTX) was sealed in a dialysis membrane and immersed in 60 mL of PBS (pH 7.4 or pH 5.5). Equal aliquots (1 mL) of PBS were collected at 0.5, 1, 2, 3, 4, 5, 6, 12, 24, 48, 72 and 85 h after dialysis, and the concentration of MTX was measured via HPLC. To test the stability of PTD/Lipo/MTX-HSA, we measured the particle size and PDI by DLS in PBS/10% FBS solution at 4°C for 7 consecutive days.

Table 1 Characterization of MTX-HSA

MTX: HSA (Molar Ratio)	Size (nm)	PDI	Zeta Potential (mV)
2:1	8.31±0.32	0.39±0.01	−14.77±3.37
4:1	10.81±0.17	0.27±0.06	−24.63±0.50
40:1	122.35±17.29	0.49±0.04	−10.25±1.30

https://doi.org/10.2147/IJN.S502850

Biocompatibility Measurement

Five hundred microliters of a 2% erythrocyte suspension prepared in saline was thoroughly mixed with 500 μL of different concentration preparations and kept at 37°C for 3 h. After centrifugation, 100 μL of the supernatant was added to a 96-well plate. Saline and ultrapure water were used as negative and positive controls, respectively. Hemoglobin released from erythrocytes was detected at 540 nm via a Varioskan Flash microplate reader (FlexStation3, USA). The hemolysis rate was calculated as follows:

$$\text{Hemolysis}(\%) = \left(A_{\text{sample}} - A_{\text{negative}}\right) / \left(A_{\text{positive}} - A_{\text{negative}}\right) \times 100\%$$

Penetration Ability of the Nanoparticles in Raw264.7 Cell Spheroids

The spheroids were prepared with Raw264.7 cells via the hanging drop/agarose method.[15] Furthermore, DID-HSA, Lipo/DID-HSA or PTD/Lipo/DID-HSA at 50 μg/mL DID were incubated with macrophage spheroids for 8 h with or without 1 mm H_2O_2, and free DID was used as a control. Images of macrophage spheroids from the top of the spheroid to the equatorial plane were obtained via Z-stack scanning via confocal laser scanning microscopy (CLSM).

Cytotoxicity Assay

The effects of nanomedicines on the viability of HUVECs, HASMCs and Raw264.7 cells were studied via the CCK-8 (Beyotime Biotechnology, cat: C0037) method. At the end of the intervention, 110 μL of CCK-8 working solution was added to each well and incubated at 37°C for 60 min. The optical density (OD) of each well was measured at 450 nm via a multifunctional enzyme marker (BioTek; Synergy H1).

Cellular Uptake of PTD/Lipo/MTX-HSA

The treated cells were then incubated with medium containing equal amounts of DID, DID-HSA, Lipo/DID-HSA, or PTD/Lipo/DID-HSA for 2 h. After rinsing, the cells were closed with sealing solution. The cells were subsequently photographed via CLSM. Similarly, cells subjected to the same treatment were harvested and then analyzed by flow cytometry via a Verse cytometer (BD Biosciences, Franklin Lakes, NJ, USA).

Assessment of the Inhibition of Foam Cell Formation

The cells were inoculated into well plates lined with sterile slides at a density of 1×10^6 cells/well, treated with each group of preparations containing 50 μg/mL of the drug, and incubated with ox-LDL (50 μg/mL) for 48 h. Subsequent operations were performed with 0.3% ORO (Beijing Solarbio Science & Technology Co., Ltd., cat: 08010) working fluid. Finally, they were all photographed for observation against a black background.

Cell Migration Assay

HASMCs in the logarithmic growth phase were inoculated in 24-well Transwell chambers at 1×10^5/well. After 24 h of treatment, the cells were removed from the chambers, rinsed and fixed with 4% paraformaldehyde for 20 min, rinsed and stained with crystal violet (Beijing Solarbio Science & Technology Co., Ltd., cat: G1062) for 15 min, rinsed and photographed under a light microscope and counted via ImageJ.

Cell Adhesion Assay

HUVECs were inoculated for 24 h. Then, THP-1 cells (CTCC, cat: SCSP-567) were fluorescently labeled with 2.5 μM BCECF (Beyotime Biotechnology; cat: C1039) in advance, the supernatant was removed by centrifugation after incubation at 37°C in the dark for 30 min, and the cells were observed under a fluorescence microscope.

Immunofluorescence (IF)

The coverslips were treated with LPS and the appropriate preparations for 24 h. After fixation, the cells were blocked and incubated with primary antibodies at 4°C overnight. The samples were incubated with the fluorescent secondary antibody and then photographed after they were blocked with blocking solution (Beyotime Biotechnology; cat: P0131).

Nuclear Plasmid Separation

The samples were collected according to the instructions of the Nuclear Protein Extraction Kit (Beijing Sola Biotechnology Co., Ltd., Item No. R0050) to obtain the extracted cell cytoplasmic proteins and nuclear proteins for denaturation, followed by WB detection.

Determination of Inflammatory Levels After Nanopreparation Treatment

Total RNA was extracted using TRIzol reagent (Solarbio Biotechnology Company, China), and cDNA was synthesized using a Vazyme cDNA RT kit (Vazyme Biotech Co., Ltd., China) according to the manufacturer's instructions. Primer sequences can be found in Table 2. QRT–PCR was performed in an ABI PRISM® 7900HT system (Applied Biosystems, USA) via SYBR Green real-time PCR Master Mix (Toyobo, Japan).

The total protein samples were extracted and then detected via Western blotting. The primary antibodies used were as follows: IL-6 (Proteintech, 21865-1-AP, 1:1000), ICAM-1 (Cell Signaling Technology, CST, cat: 67836, 1:1000), p65 (Proteintech, 66535–1, 1:1000), p-p65 (Proteintech, 82335-1-RR, 1:2000) and GAPDH (Proteintech, 60004–1, 1:50,000). The relative expression of the proteins was analyzed by the ImageJ image analysis system.

In vivo Arterial Targeting Assay

The biodistribution of PTD/Lipo/DID-HSA in the atherosclerotic vasculature was observed by randomly dividing 36 $ApoE^{-/-}$ mice into four groups (n=9 per group, 3 mice at one time point): those subjected to tail vein injection of DID, DID-HSA, Lipo/DID-HSA and PTD/Lipo/DID-HSA (0.2 mg/mL, 100 μL). The organs were removed 0.5, 6 and 24 h after injection, and the fluorescence intensity was subsequently measured on a mouse in vivo imager (PerkinElmer IVIS Lumina).

In vivo Therapeutic Efficacy of Nanoparticles

The entire segment of the aorta was exposed, and the fatty and fibrous tissue of the aorta's periphery was carefully separated, dissected longitudinally, and secured to a black sponge with a fine needle. After differentiation with 60% isopropyl alcohol, the aorta was stained with ORO (Beijing Solarbio Science & Technology Co., Ltd., cat: 08010) working fluid, and all the samples were photographed for observation against a black background. The paraffin-embedded sections were stained with H&E or Masson's trichrome and photographed.

Table 2 Primer Sequences

Gene	Forward	Reverse
IL-6 (H)	CCTGAACCTTCCAAAGATGGC	TTCACCAGGCAAGTCTCCTCA
IL-1β (H)	ATGATGGCTTATTACAGTGGCAA	GTCGGAGATTCGTAGCTGGA
ICAM-1 (H)	TTGGGCATAGAGACCCCGTT	GCACATTGCTCAGTTCATACACC
MCP-1 (H)	AGAATCACCAGCAGCAAGTGTCC	TTGCTTGTCCAGGTGGTCCATG
GAPDH (H)	ACAACTTTGGTATCGTGGAAGG	GCCATCACGCCACAGTTTC
IL-6 (M)	CTGCAAGAGACTTCCATCCAG	AGTGGTATAGACAGGTCTGTTGG
IL-1β (M)	GAAATGCCACCTTTTGACAGTG	TGGATGCTCTCATCAGGACAG
CD86 (M)	TCAATGGGACTGCATATCTGCC	GCCAAAATACTACCAGCTCACT
iNOS (M)	GTTCTCAGCCCAACAATACAAGA	GTGGACGGGTCGATGTCAC
GAPDH (M)	AGGTCGGTGTGAACGGATTTG	GGGGTCGTTGATGGCAACA

https://doi.org/10.2147/IJN.S502850

Security Testing

The collected mouse blood was left at room temperature for 30 min and centrifuged at 3000 rpm for 10 min. The serum was tested by the Laboratory Department of the Affiliated Hospital of Southwest Medical University (test indices: ALT, AST, Crea, Urea, TC, TG and LDL-c). The remaining serum was tested for IL-1β (Bioswamp, cat: MU30369), IL-6, TNF-α and IL-10 (Andygene, cat: AD3430Mo; AD3051Mo; AD2776Mo) by ELISA kits.

Statistical Analysis

The data are expressed as the mean ± standard deviation. Differences between two groups were assessed for significance by Student's *t* test, and differences between three or more groups were assessed by one-way ANOVA and Tukey's multiple comparisons test. $p<0.05$ was considered to indicate statistical significance. Histograms were constructed via GraphPad Prism software 9.0.

Results

Characterization of the PTD/Lipo/MTX-HSA Nanoparticles

Our preliminary study screened three ratios of MTX-HSA complexes with molar ratios of 2:1, 4:1 and 40:1, with particle sizes of 8.31±0.32 nm, 10.81±0.17 nm, and 122.35±17.29 nm (Table 1), respectively, and confirmed by macrophage sphere permeability experiments that the 4:1 ratio had the best penetration; thus, this ratio was chosen for subsequent experiments for the preparation of nanopreparations. As shown in Figure 1A, we first obtained MTX-HSA complexes of relatively small sizes by mixing MTX with HSA at a molar ratio of 4:1 and measured the DLE of MTX-HSA to be approximately 2.9%. Next, we prepared liposome-encapsulated MTX-HSA complexes by ethanol injection and reported that the particle size and PDI of the complexes were optimal when the mass ratio of egg yolk lecithin E80: CHEMS: PTD was 4:1:1 (Table 3). The EE of MTX was approximately 77.2%, and the corresponding DLE approached 9.8%. The obtained PTD/Lipo/MTX-HSA ruptured the sensitive liposome outer membrane in low pH and high-ROS environments, releasing the small-particle-size MTX-HSA drug (Figure 1A). A Malvern particle sizer measured the diameter of MTX-HSA at approximately 10 nm, and the diameter of PTD/Lipo/MTX-HSA was approximately 100 nm (Figure 1B). The zeta potential results indicated that the addition of PTD to the surface of Lipo/MTX-HSA resulted in a zeta potential of −29.3 mV, which helped maintain stability compared to MTX and MTX-HSA (Figure 1C). FT-IR spectroscopy was used to verify the interaction between HSA and MTX and to determine the mechanisms of drug encapsulation. The FT-IR spectra of HSA, MTX and MTX-HSA were shown in Figure 1D.

Stability Evaluation of the Nanoparticles

The stability of PTD/Lipo/MTX-HSA was also investigated after storage at 4°C in PBS and DMEM supplemented with 10% FBS. As shown, the size and PDI (Figure 1E) of PTD/Lipo/MTX-HSA remained almost unchanged for 7 consecutive days and exhibited excellent stability in vitro. We then evaluated the biocompatibility of PTD/Lipo/MTX-HSA, namely, its compatibility with red blood cells, via an in vitro hemolysis test. In this assay, we observed the transparency of the sample supernatant after incubation with PTD/Lipo/MTX-HSA (Figure S1). By counting the hemoglobin released at 540 nm, the hemolysis rate of PTD/Lipo/MTX-HSA was still well below 5%, even at a concentration of 500 μg/mL, which proved that PTD/Lipo/MTX-HSA had good biocompatibility and provided evidence of safety for further in vivo experiments (Figure 1F).

We investigated the therapeutic concentration for cell nontoxicity via the CCK-8 method. After incubation for 24 h, PTD/Lipo/MTX-HSA exhibited concentration-dependent inhibition at concentrations ranging from 0.5–100 μg/mL. Survival was still greater than 80% at a concentration of 50 μg/mL for both types of HUVECs, and significant differences were observed only at this concentration (Figure 1G). Survival was greater than 80% at a concentration of 20 μg/mL for the HASMCs (Figure 1H) and Raw264.7 cells (Figure 1I). All three cell lines presented similar trends. Therefore, we selected 50 μg/mL for the experiments on HUVECs and 20 μg/mL for the experiments on HASMCs and Raw264.7 cells. The in vivo safety details of the preparations in each group can be seen in Figure S2. No significant hepatic or renal tissue damage was seen in HE (Figure S2A) In addition, weight monitoring during the treatment period could be seen in Figure S2B, and no significant hepatic or renal damage was seen in serum tests (Figure S2C–F). Low magnification of heart, liver, spleen, lung, and kidney HE could be observed in Figure S3.

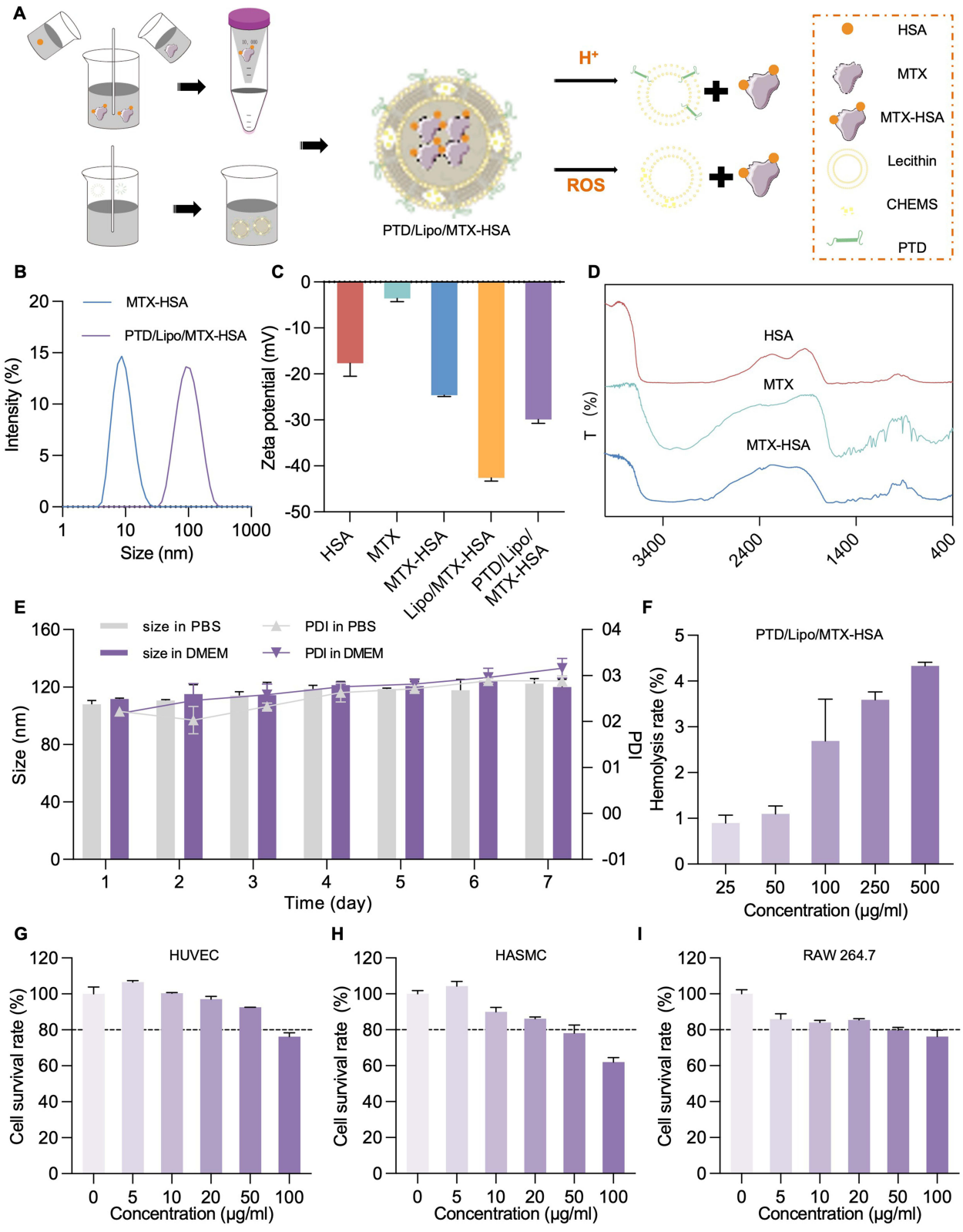

Figure 1 Characterization of the nanomaterials. (**A**). PTD/Lipo/MTX-HSA fabrication and pattern plots; (**B**) MTX-HSA and PTD/Lipo/MTX-HSA particle size plots; (**C**) Zeta potential of PTD/Lipo/MTX-HSA; (**D**) FT-IR spectra of HSA, MTX and MTX-HSA; (**E**) PTD/Lipo/MTX-HSA sequential PDI and size distributions in PBS and DMEM containing 10% FBS for 7 days; (**F**) Hemolysis plots of PTD/Lipo/MTX-HSA. (**G–I**) Results of the CCK-8 assay of PTD/Lipo/MTX-HSA-treated HUVECs, HASMCs and Raw264.7 cells.

https://doi.org/10.2147/IJN.S502850

Table 3 Characterization of PTD/Lipo/MTX-HSA

Lecithin: CHEMs:PTD (Mass Ratio)	Size (nm)	PDI	Zeta Potential (mV)
4:1:1	116.07±4.32	0.21±0.03	−19.57±0.49
4:1:2	108.73±6.45	0.31±0.05	−7.72±0.11
4:1:4	114.93±13.00	0.26±0.03	−10.63±0.61

Cumulative Drug Release of the Dual-Responsive Nanoparticles

To test the cumulative drug release properties of PTD/Lipo/MTX-HSA under different pH and H_2O_2 conditions, we first dissolved PTD/Lipo/MTX-HSA at pH 5.5, pH 5.5 with 1 mm H_2O_2, pH 7.4, and pH 7.4 with 1 mm H_2O_2 in four solvents and detected the size of the particles immediately. The largest particle size was found at pH 5.5 with 1 mm H_2O_2, which may be due to swelling of the outer membrane at 0 h (Figure 2A). We examined the particle size of the nanoparticles after 6 h in the four solvents. PTD/Lipo/MTX-HSA was approximately 10 nm in size after 6 h at pH 5.5 with H_2O_2 (Figure 2B). MTX was released much faster from PTD/Lipo/MTX-HSA at pH 5.5 with 1 mm H_2O_2, reaching 50% after 2 h and 70% after 85 h under acidic pH and high H_2O_2 conditions but < 40% even after 85 h at pH 7.4, suggesting its dual-responsive properties (Figure 2C). TEM images revealed that PTD/Lipo/MTX-HSA nanoparticles ruptured in a weakly acidic and high-ROS environment and could release small-sized MTX-HSA nanoparticles on demand (Figure 2D). Thus, the homogeneous PTD/Lipo/MTX-HSA was regularly spherical with an average particle size of approximately 100 nm in a neutral environment at pH 7.4 and showed no significant changes after 0 and 6 h. In contrast, the most rapid membrane rupture was observed at pH 5.5 and in the presence of 1 mm H_2O_2 (Figure 2E). Simple pattern plot of pH- or ROS-responsive PTD/Lipo/MTX-HSA (Figure 2F).

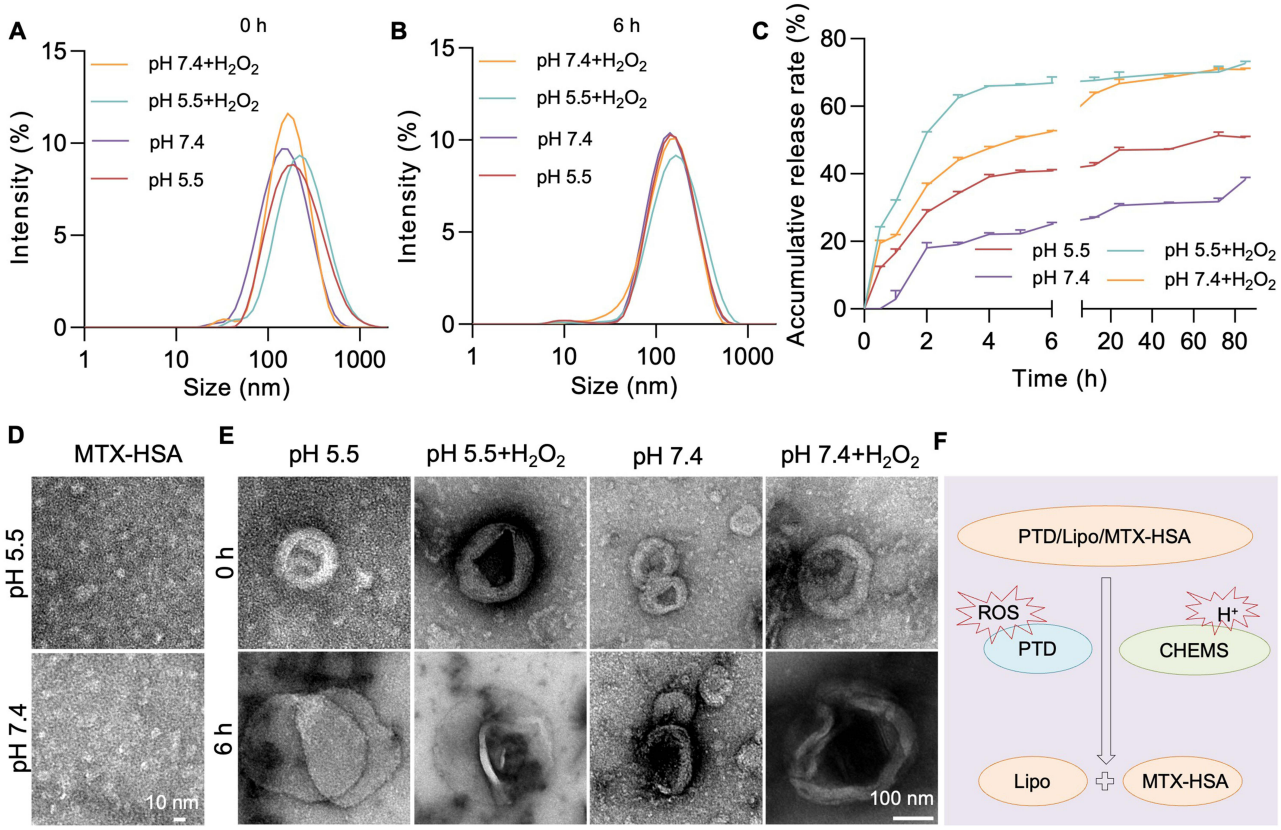

Figure 2 Dual responsiveness of nanoparticles to pH and ROS. (**A**) Particle size of PTD/Lipo/MTX-HSA under different conditions at 0 h; (**B**) Particle size of PTD/Lipo/MTX-HSA under different conditions at 6 h; (**C**) Drug release rate of PTD/Lipo/MTX-HSA under different conditions; (**D**) TEM of MTX-HSA at pH 5.5 and pH 7.4 (scale 10 nm); (**E**) TEM of PTD/Lipo/MTX-HSA at pH 5.5 and pH 7.4 with/without 1 mm H_2O_2 at 0 and 6 h (scale 100 nm); (**F**) Schematic diagrams of different environments.

Cellular Uptake Evaluation

For in vitro experiments, we used Raw264.7 cells stimulated with LPS as a model to study the cellular uptake of PTD/Lipo/MTX-HSA by macrophages via CLSM. DID labeling was used to trace the intracellular fate of PTD/Lipo/DID-HSA, and the cellular location was revealed by DAPI staining. LPS-stimulated Raw264.7 cells were incubated with DID, DID-HSA, Lipo/DID-HSA or PTD/Lipo/DID-HSA for 2 h. Figure 3A and C showed that the intensity of red fluorescence in the LPS-activated

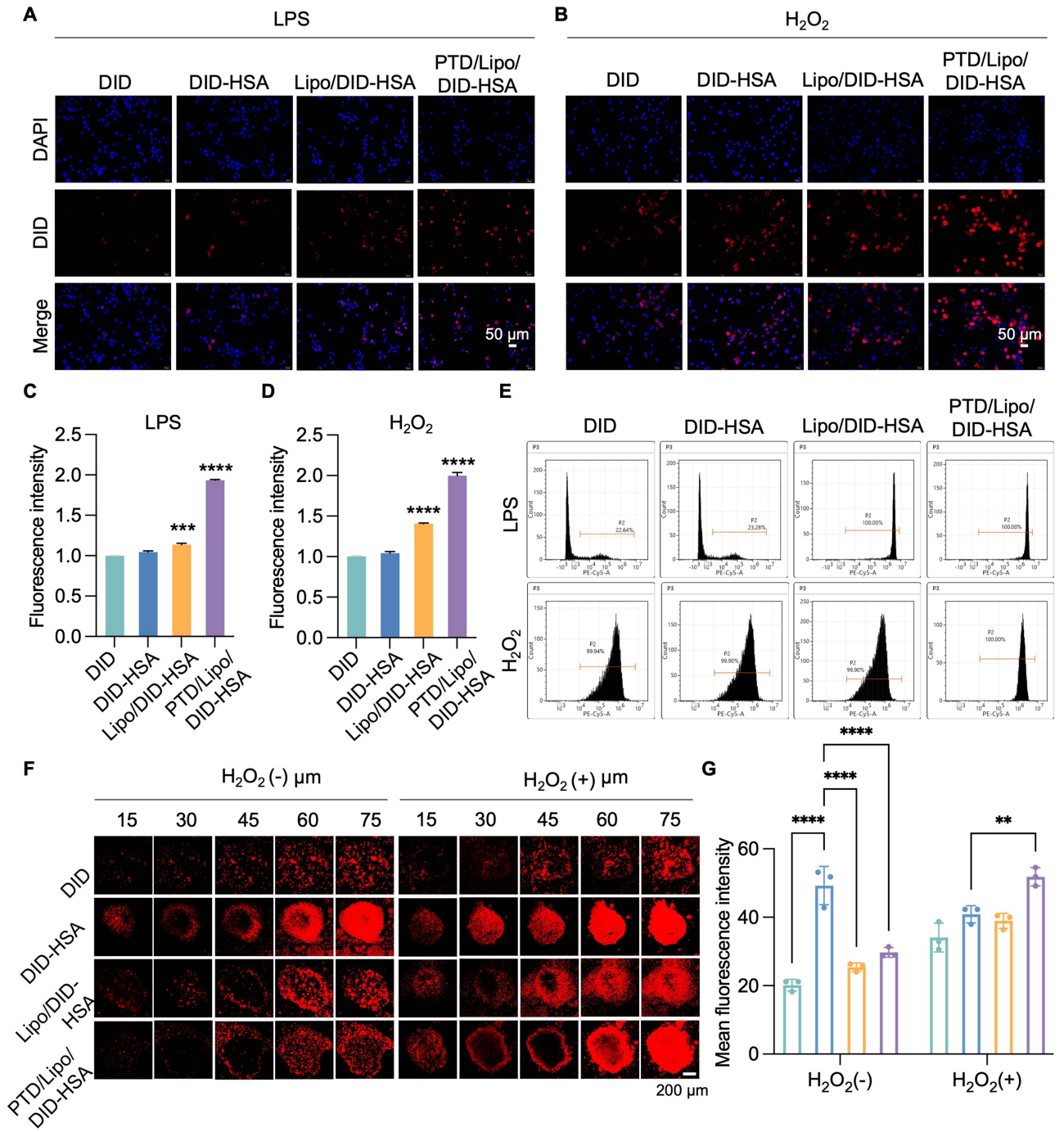

Figure 3 In vitro targeting of nanomaterials. (**A** and **B**) are the confocal microscopy results of DID, DID-HSA, Lipo/DID-HSA and PTD/Lipo/DID-HSA in the presence of LPS or H_2O_2, respectively (scale 50 μm); (**C**) Fluorescence statistics for A; (**D**) Fluorescence statistics for B; (**E**) Flow cytometry results of DID, DID-HSA, Lipo/DID-HSA and PTD/Lipo/DID-HSA in the presence of LPS or H_2O_2, respectively; (**F**) Fluorescence penetration efficiency of different formulations in Raw264.7 cell spheroids at 8 h (scale 200 μm); (**G**) The fluorescence statistics at 75 μm of F. (***<0.001 vs DID; ****<0.0001 vs DID).

https://doi.org/10.2147/IJN.S502850

Raw264.7 cells in the PTD/Lipo/DID-HSA group was significantly greater than that in the other three groups. In Raw264.7 cells stimulated with H_2O_2 (Figure 3B and D), the fluorescence intensity in the PTD/Lipo/DID-HSA group was greater than that in the other three groups. These results suggested that PTD/Lipo/DID-HSA could be internalized more by the dual-activated Raw264.7 cells, which was consistent with the fluorescence intensity data obtained via flow cytometry (Figure 3E).

PTD/Lipo/DID-HSA Demonstrates an Efficient Ability for Deeper Penetration Into Macrophage Spheroids

In fluorescent DID-loaded nanoparticles penetration assessment, macrophage spheroids were utilized to mimic 3D structure of atherosclerotic plaque tissue and the penetration behaviors were evaluated by using CLSM (Figure 3F and G). Compared with free DID, DID-HSA showed the highest penetration ability among all the tested groups probably ascribed to its small size. Notably, Lipo/DID-HSA and PTD/Lipo/DID-HSA were much lower in the deeper part of the macrophage spheroids than in the DID-HSA group, possibly because the large particles limited their permeability. ROS-responsive PTD/Lipo/DID-HSA nanoparticle penetrated deeper in macrophage spheroids than Lipo/DID-HSA. Nonetheless, such behavior difference in penetration was not seen in the absence of H_2O_2. The result ascertained that PTD/Lipo/DID-HSA rapidly disassembled in response to the presence of H_2O_2 and released smaller DID-HSA that penetrated deeper in the macrophage spheroids.

Antifoam Effect of PTD/Lipo/MTX-HSA on Cell Formation in Vitro

We induced myogenic foam cells with ox-LDL in HASMCs, and oil red O staining revealed large areas of red staining, which were reduced after MTX, MTX-HSA, Lipo/MTX-HSA and PTD/Lipo/MTX-HSA treatment compared with those in the ox-LDL group (Figures 4A, B and S4). Both Lipo/MTX-HSA and PTD/Lipo/MTX-HSA were more effective than MTX, while PTD/Lipo/MTX-HSA had the greatest effect. We induced HASMCs in an inflammatory environment with LPS, and compared with those in the LPS group, the number of cells that crossed the Transwell chambers decreased, and purple staining decreased after the MTX, MTX-HSA, Lipo/MTX-HSA and PTD/Lipo/MTX-HSA treatments (Figure 4C and D); in addition, it was more effective in the MTX-HSA, Lipo/MTX-HSA and PTD/Lipo/MTX-HSA groups than in the MTX-treated group. Compared with the LPS group, the PTD/Lipo/MTX-HSA group had the lowest number of cells. Endothelial-monocyte adhesion is not only the earliest process in the development of atherosclerosis but also essential for late plaque formation.[16] We used a cellular model of inflammation caused by LPS-induced HUVEC and stained monocytes THP-1 with BCECF probe, and the number of monocytes adhering to the surface of endothelial cells was reduced by MTX, MTX-HSA, Lipo/MTX-HSA, and PTD/Lipo/MTX-HSA treatments compared to the LPS group (Figure S5A), and the PTD/Lipo /MTX-HSA group had the lowest number of cells. The statistical graphs are shown in (Figure S5B).

Anti-Inflammatory Effects of PTD/Lipo/MTX-HSA in Vitro

In vivo, we subjected the serum from five groups of animals to ELISA. IL-1β, IL-6 and TNF-α results revealed that the levels of IL-1β, IL-6 and TNF-α in the MTX-HSA, Lipo/MTX-HSA and PTD/Lipo/MTX-HSA groups were lower than those in the saline group, and the levels of IL-1β and TNF-α in the MTX group were lower (Figure 5A–C). In particular, the decrease in TNF-α was greater in both the Lipo/MTX-HSA and PTD/Lipo/MTX-HSA groups than in the MTX-treated group. The statistical analysis of the anti-inflammatory cytokine IL-10 suggested that it was mostly elevated in the PTD/Lipo/MTX-HSA groups compared with the saline group (Figure 5D). The level of the anti-inflammatory index IL-10 in the PTD/Lipo/MTX-HSA group was greater than that in the model group, suggesting that the nanoparticles had a dominant attenuating effect on the level of inflammation in atherosclerosis.

For in vitro experiments, we used LPS-activated HUVECs as an inflammatory cell model. LPS stimulation leads to increased secretion of proinflammatory cytokines, including TNF-α, IL-1β and IL-6.[17–19] Therefore, we treated HUVECs with LPS, LPS+MTX, LPS+MTX-HSA, LPS+Lipo/MTX-HSA or LPS+PTD/Lipo/MTX-HSA for 24 h. The mRNA expression of IL-6, IL-1β, MCP-1 and ICAM-1 was measured via qRT–PCR (Figure 5E–H). The results suggested a significant increase in inflammation in the LPS group compared with the control group. There was a significant reduction in the expression of IL-6 in the LPS+Lipo/MTX-HSA and LPS+PTD/Lipo/MTX-HSA groups compared with that in the

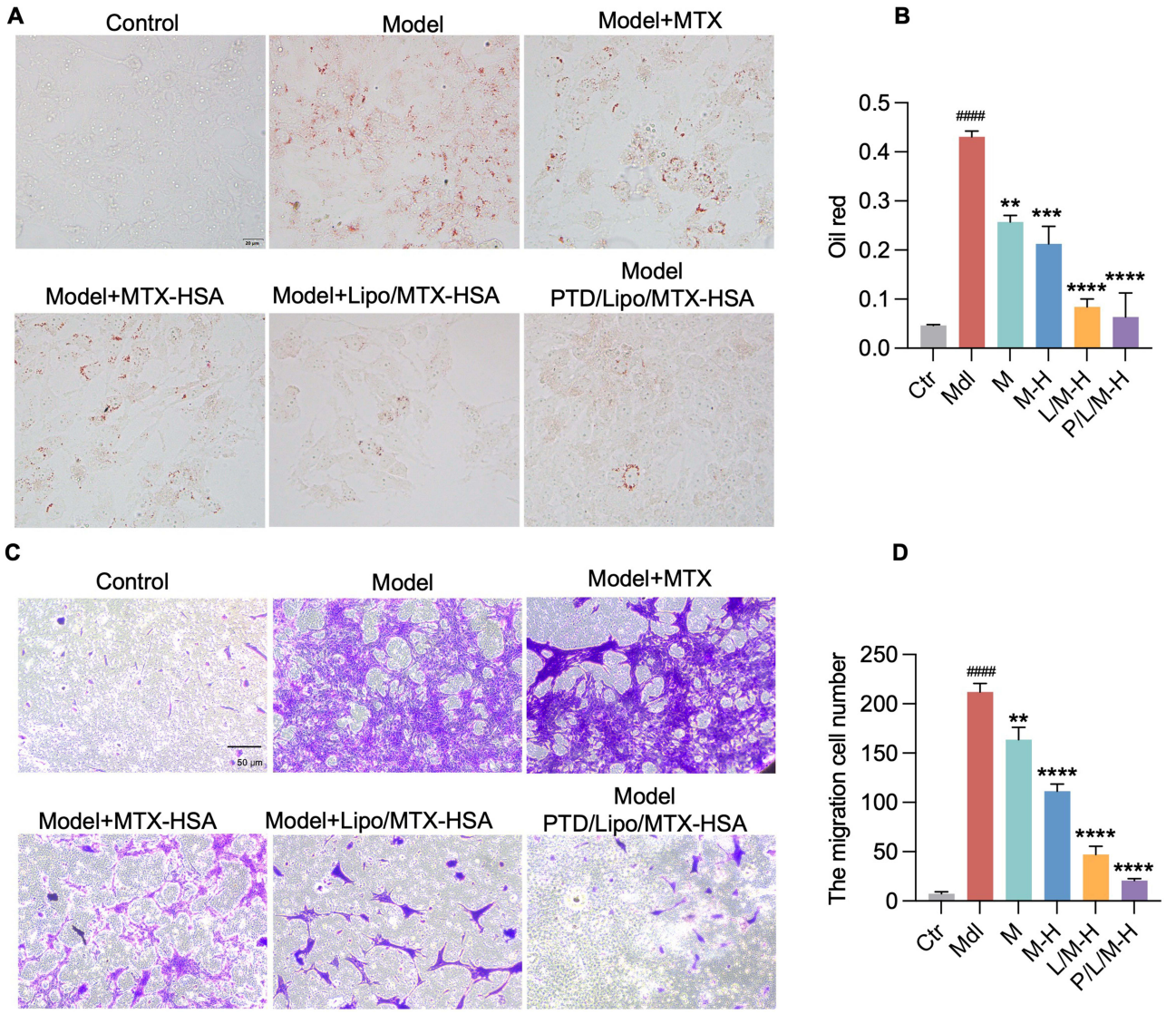

Figure 4 Antilipid uptake effects of the nanomaterials in vitro. (**A**) The control, model (ox-LDL), ox-LDL+MTX, ox-LDL+MTX-HSA, ox-LDL+Lipo/MTX-HSA and ox-LDL+PTD/Lipo/MTX-HSA preparations were treated with HASMCs, and white light imaging of oil red O staining was performed (scale 20 μm); (**B**) is a statistical graph of A; (**C**) The control, model (LPS), LPS+MTX, LPS+MTX, LPS+MTX-HSA, LPS+Lipo/MTX-HSA and LPS+PTD/Lipo/MTX-HSA groups were treated with HASMCs and stained with crystal violet. Images were taken under an optical microscope (scale 50 μm). (**D**) is a statistical graph of C. (Ctr, control; Mdl, model (LPS/ox-LDL); M, model+MTX; M-H, model+MTX-HSA; L/M-H, model+Lipo/MTX-HSA; P/L/M-H, model+PTD/Lipo/MTX-HSA; ####<0.0001 vs control; *<0.05; **<0.01; ***<0.001; ****<0.0001 vs Model).

LPS group; for IL-1β, all four preparations were obviously reduced after treatment compared with those in the LPS group. The use of different MTX-HSA formulations for 24 h resulted in substantial inhibition of LPS-induced cytokine expression. PTD/Lipo/MTX-HSA exhibited the most effective anti-inflammatory effect, which could be attributed to its enhanced ability to clear ROS. The adhesion molecule ICAM-1 recruits inflammatory cells to the endothelium, thus participating in the development and progression of atherosclerosis.[20] Previous studies have shown that blocking ICAM-1 has an antiatherosclerotic effect.[21,22] In contrast, the levels of the endothelial cell adhesion indicator MCP-1 were dramatically lower after treatment with the four groups of preparations than after treatment with the LPS group; in particular, the levels in the LPS+PTD/Lipo/MTX-HSA group were greater than those in the other groups. The expression of the adhesion molecule ICAM-1 was lower in the latter three preparations than in the LPS group and was more strongly affected than that in the MTX treatment group. The results of the detection of the adhesion molecules MCP-1 and ICAM-1 in HUVECs also suggested that PTD/Lipo/MTX-HSA had the greatest antiadhesion ability.

https://doi.org/10.2147/IJN.S502850

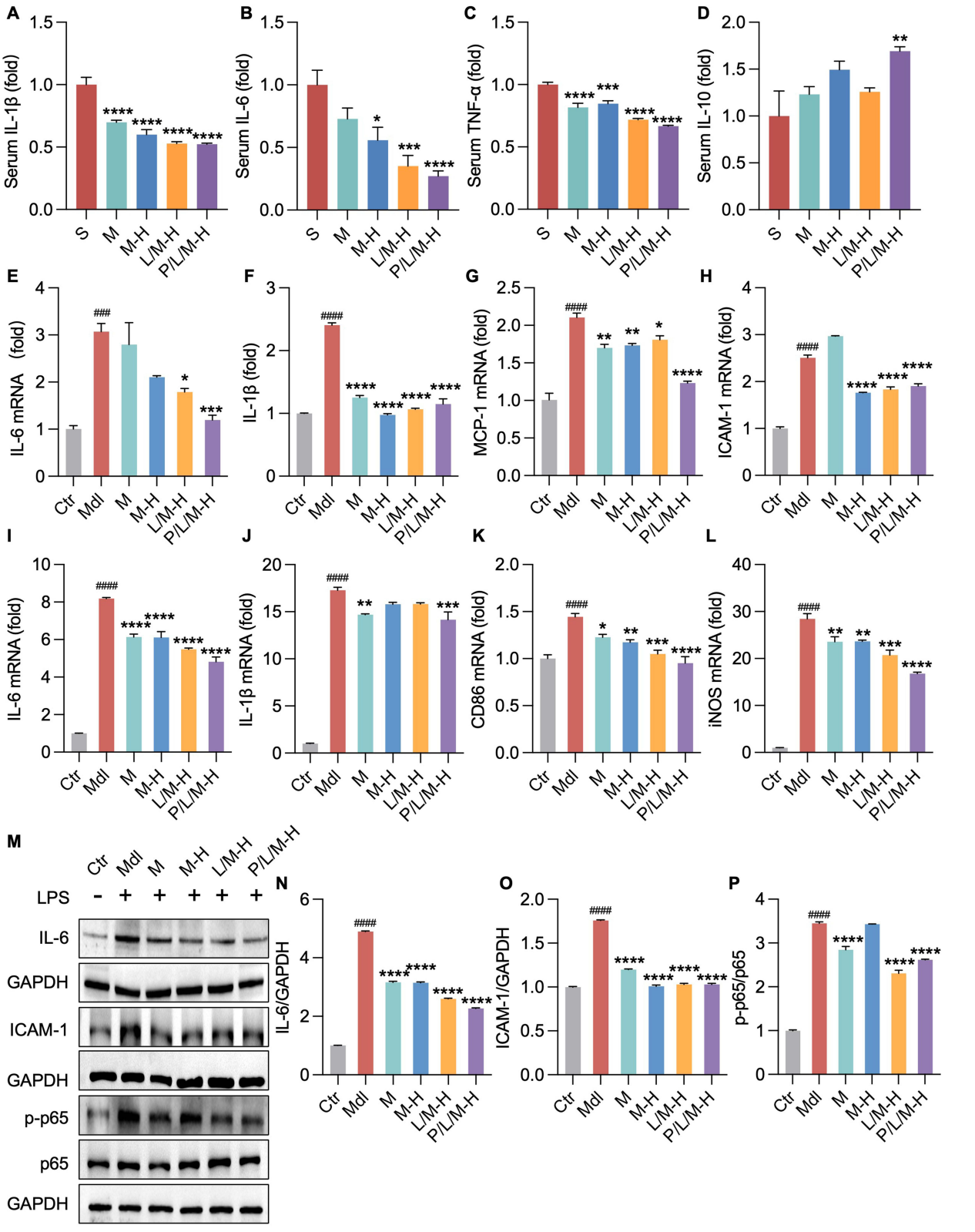

Figure 5 Anti-inflammatory effects of the nanomaterials in vitro. (**A**), (**B**), (**C**) and (**D**) are the ELISA results for serum IL-1β, IL-6, TNF-α and IL-10, respectively. (S, saline; M, MTX; M-H, MTX-HSA; L/M-H, Lipo/MTX-HSA; P/L/M-H, PTD/Lipo/MTX-HSA; *<0.05; **<0.01; ***<0.001; ****<0.0001 vs saline); E, F, G, H are the PCR results for the control, model (LPS), LPS+MTX, LPS+MTX-HSA, LPS+Lipo/MTX-HSA and LPS+PTD/Lipo/MTX-HSA-treated HUVECs ((**E**), IL-6; (**F**), IL-1β; (**G**), MCP-1; (**H**), ICAM-1); (**I**–**L**) are the PCR results for the control, LPS, LPS+MTX, LPS+MTX-HSA, LPS+Lipo/MTX-HSA and LPS+PTD/Lipo/MTX-HSA-treated Raw264.7 cells ((**I**), IL-6 (**J**), IL-1β; (**K**), CD86; (**L**), iNOS); (**M**) shows the WB results; (**N**) (IL-6), (**O**) (ICAM-1) and (**P**) (p-p65/p65) are the statistical plots of I. (Ctr, control; Mdl, model; M, model+MTX; M-H, model+MTX-HSA; L/M-H, model+Lipo/MTX-HSA; P/L/M-H, model+PTD/Lipo/MTX-HSA; ####<0.001; #####<0.0001 vs control; *<0.05; **<0.01; ***<0.001; ****<0.0001 vs Model).

Macrophages are key cells involved in the inflammatory response, and they differentiate into the M1 type under the stimulation of inflammatory factors, accompanied by increased expression of the markers CD86 and iNOS. LPS-treated Raw264.7 cells presented increased expression of the inflammatory factors IL-6 and IL-1β at the mRNA level, as well as increased expression of the M1 biomarkers CD86 and iNOS (Figure 5I–L). All four formulations reduced the expression of the inflammatory factor IL-6 and the M1 biomarkers CD86 and iNOS. PTD/Lipo/MTX-HSA significantly decreased the IL-1β concentration compared with that in the LPS group. Compared with the MTX and Lipo/MTX-HSA formulations, the PTD/Lipo/MTX-HSA formulation reduced the levels of IL-6 and iNOS, suggesting that it had the most significant anti-inflammatory effects.

Anti-Inflammatory Effects of PTD/Lipo/MTX-HSA via the p65 Pathway in the Treatment of AS

We examined the improvement in the classical inflammatory signal IL-6 induced by four agents at the protein level in a cellular inflammation model of LPS-induced HUVECs. The protein imprint map was shown in Figure 5M. According to the protein analysis, the LPS group presented significantly greater levels of these proteins than did the control group did, while the levels in the LPS+PTD/Lipo/MTX-HSA groups were lower than those in the LPS group were (Figure 5N). The expression of ICAM-1, a classical HUVEC adhesion molecule, was significantly greater in the LPS group than in the control group, and the expression in the remaining four groups decreased (Figure 5O). To explore the possible pathway through which PTD/Lipo/MTX-HSA affects AS, we tested classical p-p65/p65, which was substantially greater in the LPS group than in the control group and decreased more in the LPS+PTD/Lipo/MTX-HSA groups than in the LPS group (Figure 5P). Our experimental results confirmed that PTD/Lipo/MTX-HSA induced LPS-induced inflammatory responses, possibly through the p65 pathway.

P65 is a key transcription factor in the inflammatory response, and when p65 is phosphorylated and activated, it enables the expression of target genes. When blood vessels suffer from chronic inflammation, activated p65 acts as a nuclear transcription factor, initiating the inflammatory response and exacerbating vascular inflammation. In the control group, p65 was located mostly in the cytoplasm and nucleus. P65 entry into the nucleus increased after 12 h of LPS stimulation, and its expression was obvious in the nucleus. Interestingly, after treatment with different formulations, PTD/Lipo/MTX-HSA mostly inhibited the translocation of p65 and had a more significant effect than the other treatments did (Figure 6A). At the protein level, we obtained similar results (Figure 6B and C). PTD/Lipo/MTX-HSA markedly reduced the amount of p65 that entered the nucleus in LPS-induced macrophages.

Evaluation of the Targeting Ability of Nanoparticles

First, we successfully established an animal model according to the classical atherosclerosis modeling approach by feeding ApoE$^{-/-}$ mice a high-fat diet. To assess the biodistribution of the final formulation in vivo, we administered the DID, DID-HSA, Lipo/DID-HSA or PTD/Lipo/DID-HSA formulation to ApoE$^{-/-}$ mice via tail vein injection. IVIS was used to image isolated organs 0.5, 6 or 24 h after injection (Figure 7A and B). Compared with that in the DID group, the fluorescence accumulation of PTD/Lipo/DID-HSA in the vasculature increased over time ($p<0.05$) and was most pronounced at 24 h. The results suggested that PTD/Lipo/DID-HSA circulated longer in vivo and accumulated more in the vasculature than did the DID, DID-HSA and Lipo/DID-HSA groups did, ie, the PTD/Lipo/DID-HSA groups presented longer retention times at atherosclerotic sites. Our results revealed that the formulation could prolong the circulation time, and PTD could respond intelligently to high-ROS environments, and CHEMS could respond to pH, which was key to precisely targeting and controlled release of small nanoparticles for penetrating thick fiber caps (Figure 7C and D). Statistics for the other organs can be viewed in Figure S7.

In vivo Therapeutic Efficiency of PTD/Lipo/MTX-HSA

A flowchart of the animal experiments is shown in Figure S6A. To better observe the therapeutic effects of the preparations, we excised the ascending aorta to the bilateral common iliac arteries and performed macroscopic oil red O staining, which revealed that all four preparations reduced the number of plaques on the arterial wall (Figure 7E and F), with PTD/Lipo/MTX-HSA

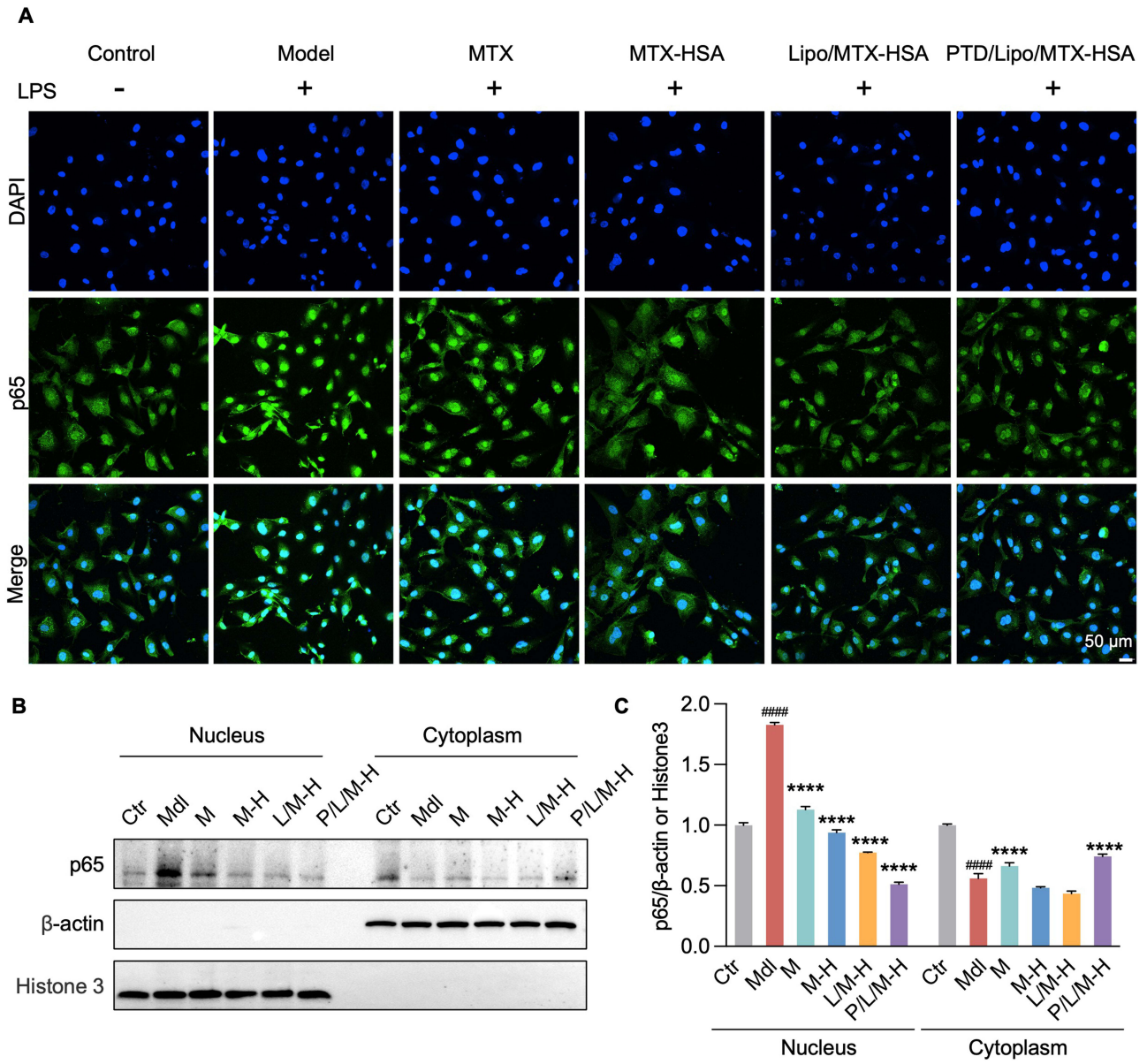

Figure 6 Anti-inflammatory pathway of nanomaterials in vitro. (**A**) Control, model (LPS), LPS+MTX, LPS+MTX-HSA, LPS+Lipo/MTX-HSA, and LPS+PTD/Lipo/MTX-HSA groups for immunofluorescence imaging; DAPI is shown in blue; p65 is shown in green; merge is the combination of the two (scale 50 μm); (**B**) shows the WB results; (**C**) is the statistical plot of B. (Ctr, control; Mdl, model; M, model+MTX; M-H, model+MTX-HSA; L/M-H, model+Lipo/MTX-HSA; P/L/M-H, model+PTD/Lipo/MTX-HSA; ####<0.0001 vs the control; ****<0.0001 vs model).

showing the best therapeutic effect. Cross-sectional HE staining of the plaques may reveal the most pronounced plaque reduction in PTD (Figure S6B). Moreover, we performed TC, TG, and LDL-c assays on serum samples, and the results revealed that both MTX-HSA and PTD/Lipo/MTX-HSA reduced lipid TC and TG levels in AS-diseased mice (Figure 7G and H). The serum LDL-c levels were lower in all four preparations than in the saline-injected group (Figure 7I). On the basis of the serum lipid results, all four nanoparticles favored lipid metabolism in AS mice, with Lipo/MTX-HSA and PTD/Lipo/MTX-HSA showing the best lipid-lowering effects. In particular, the lipid-lowering effect in the PTD/Lipo/MTX-HSA group was significantly greater than that in the MTX group. H&E staining of the aorta (Figure S6B) indicated that all four nanoparticle groups had fewer atheromatous plaques than did the saline group, with PTD/Lipo/MTX-HSA having the greatest effect.

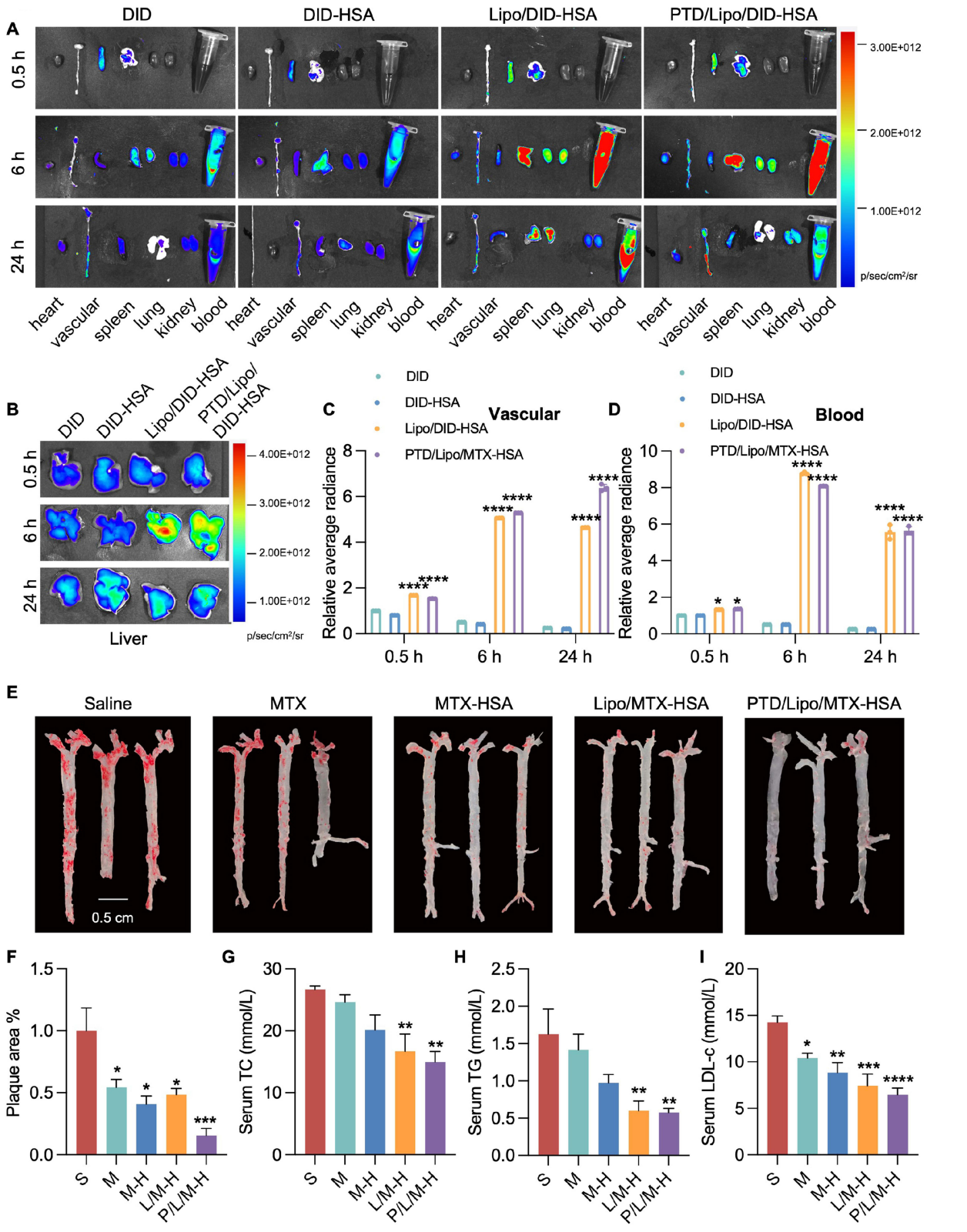

Figure 7 In vivo targeting and antilipidemic effects of the nanomaterials. (**A**). In vivo heart, vascular, spleen, lung, kidney and blood imaging thermograms of DID, DID-HSA, Lipo/DID-HSA and PTD/Lipo/DID-HSA at 0.5, 6 and 24 h. (**B**) In vivo liver imaging thermograms of DID, DID-HSA, Lipo/DID-HSA and PTD/Lipo/DID-HSA at 0.5, 6 and 24 h. (**C** and **D**). Statistical graphs of vascular and blood images. (*<0.05 vs DID; ****<0.0001 vs DID); (**E**) Oil red O staining of whole sections after treatment with saline, MTX, MTX-HSA, Lipo/MTX-HSA and PTD/Lipo/MTX-HSA (scale 0.5 cm); (**F**) Statistical diagram of vascular plaques; (**G**), (**H**) and (**I**) are the serum TC, TG and LDL-c results of in vivo experiments with saline, MTX, MTX-HSA, Lipo/MTX-HSA and PTD/Lipo/MTX-HSA preparations, respectively (S, saline; M, MTX; M-H, MTX-HSA; L/M-H, Lipo/MTX-HSA; P/L/M-H, PTD/Lipo/MTX-HSA; *<0.05; **<0.01; ***<0.001; ****<0.0001 vs saline).

https://doi.org/10.2147/IJN.S502850

Discussion

It is well known that proinflammatory factors are among the most important inflammatory triggers during AS episodes; they induce inflammatory cell infiltration in the vascular wall and oxidative stress in defense cells, leading to the production of intracellular ROS.[23,24] The use of anti-inflammatory drugs is a promising approach for the management of this inflammatory disease. However, currently used anti-inflammatory drugs are limited by insufficient efficacy and increased risk of serious infections and malignancies,[25–27] and drug delivery systems are needed to reduce nontargeted side effects and improve therapeutic efficacy. Recently, some studies have been conducted on nanoparticles designed for high-ROS or weakly acidic inflammatory environments to control the release of drug-carrying agents in the inflammatory microenvironment.[28] However, single responsive nanomedicines may not be sufficiently responsive to the inflammatory environment, resulting in inadequate or delayed drug release. SV MC@RBCs were prepared on the basis of AS-localized ROS and high shear stress dual-sensitive NPs composed of poly (glycidyl methacrylate)-polypropylene sulfide (PGED-PPS). The preparation could react with excess ROS to become hydrophilic, thereby forcing the micelles to rupture, leading to on-demand drug release and enabling synergistic treatment of atherosclerosis with drugs and materials.[29]

Considering the overproduction of ROS and H^+ at the site of inflammation, the rational design of a ROS and pH dual-sensitive size-adjustable drug delivery system could release drugs on demand by responding to inflammatory stimuli at the site of plaque sites and further improve therapeutic efficacy in vitro and in vivo, revealing a promising anti-inflammatory approach. The TK functional group burst can respond to ROS in the ischemic environment by rapidly cleaving them to nontoxic thiol and acetone products that can cleave the TK-containing PTD.[30] In this study, we designed a dual-sensitive PTD/Lipo/MTX-HSA system by modifying PTD with our previously prepared smart Lipo/MTX-HSA system. The results of in vitro accumulation drug experiments revealed that PTD/Lipo/MTX-HSA had more sensitive drug release properties under high-ROS and low-pH conditions. In addition, the preparation reduced the levels of inflammatory factors and decreased the expression of M1-type markers in Raw264.7 cells. The in vivo biodistribution results showed that the formulation could prolong the circulation time in the bloodstream and thus enhance the accumulation of the site of inflammation. Furthermore, the results demonstrated that PTD/Lipo/MTX-HSA not only targeted the site of inflammation but also reduced the levels of inflammatory factors in dysfunctional cells, suggesting that PTD/Lipo/MTX-HSA had a better ability to penetrate deeper into plaques. The vascular immunohistochemistry results of the in vivo experiments statistically revealed a significant reduction in the number of vascular inflammatory smooth muscle cells and macrophages, which might indicate a more precise targeting and penetration effect of PTD/Lipo/MTX-HSA as well as more controllable drug release. To better explore the mechanism of action of the NPs, we explored the classical inflammatory pathway p65 and found that PTD/Lipo/MTX-HSA inhibits the entry of p65 into the nucleus. This reduces the production of inflammatory factors. The literature suggests that MTX decreases basal levels of NF-κB activity by increasing lincRNA-p21 levels through a DNA-dependent protein kinase catalytic subunit (DNA PKcs)-dependent mechanism.[31] Spurlock et al discovered MTX inhibited activation of NF-κB via depletion of tetrahydrobiopterin (BH4) and increased Jun-N-terminal kinase (JNK)-dependent p53 activity.[32] These suggest that PTD/Lipo/MTX-HSA can inhibit NF-κB p65 to act.

The natural biomimetic nanodelivery system of HSA has the advantages of better biocompatibility, low cytotoxicity and nonimmunogenicity. In our study, as a highly biocompatible agent, HSA can be used for assembly with MTX to prepare small complexes for better penetration of deeper plaques. The encapsulation of small MTX-HSA complexes in ROS and pH-sensitive liposomes not only resolved the retention of small nanoparticles in the bloodstream but also allowed the efficient accumulation of nanoparticles in inflamed tissues. Furthermore, the released small nanoparticles could penetrate the macrophage spheres to reduce their foaming. The PTD/Lipo/MTX-HSA system intelligently targets inflammatory sites, allowing it to act on other inflammatory sites in the body, such as those involved in rheumatoid arthritis, chronic pancreatitis or chronic gastritis. The lack of long-term safety and efficacy data from large animal models is a shortcoming of our experiments. Additionally, potential off-target effects and immune responses to nanoparticles should be investigated to further assess their safety for use.

A recent study revealed that VSMCs had multiple characteristics related to tumor cell biology and that their "phenotypic switching" played a central role in AS development and complications, revealing that AS is a tumor-like disease. To this end, future research should focus on inhibiting the malignant proliferation and migration of VSMCs and preventing their phenotypic transformation. Additionally, subsequent more detailed study of the mechanisms by which nanoparticles penetrate deeper into the plaque and suppress inflammation is also needed as to fully understand their mode of action. In addition, there

is a complex inflammatory network between VSMCs and macrophages,[33] and our preparation should be further modified with specific targeted ligands to precisely inhibit this inflammatory loop between tissue cells and immune cells, which could lead to the development of novel precision targeting strategies for treating atherosclerotic cardiovascular disease.

Conclusion

In conclusion, we successfully developed a size-controlled PTD/Lipo/MTX-HSA that responded to an inflammatory oxidative and acidic microenvironment. The results showed that the nanoparticles displayed good systemic circulatory properties and significantly aggregated in plaque locations, with controlled release of small-particle-sized MTX-HSA by ROS and a pH dual response in the inflammatory microenvironment. Small complex nanoparticles could penetrate deeply into the injured endothelium, reaching damaged smooth muscle cells and macrophages and achieving synergistic inhibitory effects on migration ability and inflammation, respectively. PTD/Lipo/MTX-HSA exhibited precise targeting and on-demand drug release properties for dysfunctional plaque depth accumulation and favorable anti-inflammatory effects both in vitro and in vivo, providing a practical platform for the treatment of AS.

Data Sharing Statement

All the data needed to support the conclusions are presented in the paper or the additional materials.

Acknowledgments

All the authors are grateful for assistance from the following research platforms: the Noncoding Key Laboratory, Southwest Medical University; the Public Platform of Advanced Detecting Instruments, Public Center of Experimental Technology, Southwest Medical University; and the School of Pharmacy at Southwest Medical University (Luzhou, Sichuan).

Author Contributions

All authors made a significant contribution to the work reported, whether that was in the conception, study design, execution, acquisition of data, analysis and interpretation, or in all these areas; took part in drafting, revising or critically reviewing the article; gave final approval of the version to be published; had agreed on the journal to which the article had been submitted; and agreed to be accountable for all aspects of the work.

Funding

This work was supported by the National Natural Science Foundation of China (Grant No. 82170459), the Special Project on the Central Guided Local Science and Technology Development of Sichuan Province (2022ZYD0061), the Innovation Special Project of Sichuan Provincial Department of Science and Technology - Project (2022YFS0627) and the Suining First People's Hospital-Southwest Medical University Cooperation Project (2022SNXNYD06).

Disclosure

The authors have declared no conflicts of interest in this work.

References

1. Yuan J, Li L, Yang Q, et al. Targeted treatment of ischemic stroke by bioactive nanoparticle-derived reactive oxygen species responsive and inflammation-resolving nanotherapies. *ACS Nano*. 2021;15:16076.
2. Hu R, Dai C, Dong C, et al. Living Macrophage-Delivered Tetrapod PdH Nanoenzyme for Targeted Atherosclerosis Management by ROS Scavenging, Hydrogen Anti-inflammation, and Autophagy Activation. *ACS Nano*. 2022;16(10):15959. doi:10.1021/acsnano.2c03422
3. Jain T, Nikolopoulou EA, Xu Q, Qu A. Hypoxia inducible factor as a therapeutic target for atherosclerosis. *Pharmacol Ther*. 2018;183:22. doi:10.1016/j.pharmthera.2017.09.003
4. Pan H, Ho SE, Xue C, et al. Atherosclerosis is a smooth muscle cell–driven tumor-like disease. *Circulation*. 2024;2024:1.
5. Bennett MR, Sinha S, Owens GK. Vascular Smooth Muscle Cells in Atherosclerosis. *Circ Res*. 2016;118(4):692. doi:10.1161/CIRCRESAHA.115.306361
6. Devel L, Almer G, Cabella C, et al. Biodistribution of Nanostructured Lipid Carriers in Mice Atherosclerotic Model. *Molecules*. 2019;24(19):3499. doi:10.3390/molecules24193499
7. Ou HX, Guo BB, Liu Q, et al. Regulatory T cells as a new therapeutic target for atherosclerosis. *Acta Pharmacol Sin*. 2018;39(8):1249. doi:10.1038/aps.2017.140

8. Pontarollo G, Kiouptsi K, Reinhardt C. A holobiont view on thrombosis: unravelling the microbiota's influence on arterial thrombus growth. *Microb Cell*. 2020;7(1):28. doi:10.15698/mic2020.01.704
9. Zhang J, Zu Y, Dhanasekara CS, et al. Detection and treatment of atherosclerosis using nanoparticles. *Wiley Interdiscip Rev Nanomed Nanobiotechnol*. 2017;9:e1412
10. Lobatto ME, Calcagno C, Millon A, et al. Atherosclerotic Plaque Targeting Mechanism of Long-Circulating Nanoparticles Established by Multimodal Imaging. *ACS Nano*. 2015;9(2):183. doi:10.1021/nn506750r
11. Kumar D, Pandit R, Yurdagul Jr A. Mechanisms of continual efferocytosis by macrophages and its role in mitigating atherosclerosis. *Immunometabolism*. 2023;5(1):e00017. doi:10.1097/IN9.0000000000000017
12. Bhogal RH, Curbishley SM, Weston CJ, Adams DH, Afford SC. Reactive oxygen species mediate human hepatocyte injury during hypoxia/reoxygenation. *Liver Transpl*. 2010;16(11):1303. doi:10.1002/lt.22157
13. He J, Zhang W, Zhou X, et al. Reactive oxygen species (ROS)-responsive size-reducible nanoassemblies for deeper atherosclerotic plaque penetration and enhanced macrophage-targeted drug delivery. *Bioact Mater*. 2023;19:115. doi:10.1016/j.bioactmat.2022.03.041
14. Zheng X, Yang H, Zhang Z, et al. pH-responsive size-adjustable liposomes induce apoptosis of fibroblasts and macrophages for rheumatoid arthritis treatment. *Acta Biomater*. 2024;2024:1.
15. Zhang W, Li C, Baguley BC, et al. Optimization of the formation of embedded multicellular spheroids of MCF-7 cells: how to reliably produce a biomimetic 3D model. *Anal Biochem*. 2016;515:47. doi:10.1016/j.ab.2016.10.004
16. Combadiere C, Potteaux S, Rodero M, et al. Combined Inhibition of CCL2, CX3CR1, and CCR5 Abrogates Ly6C hi and Ly6C lo Monocytosis and Almost Abolishes Atherosclerosis in Hypercholesterolemic Mice. *Circulation*. 2008;117(13):1649. doi:10.1161/CIRCULATIONAHA.107.745091
17. Shapouri-Moghaddam A, Mohammadian S, Vazini H, et al. Macrophage plasticity, polarization, and function in health and disease. *J Cell Physiol*. 2018;233(9):6425. doi:10.1002/jcp.26429
18. Zhang P, Yang M, Chen C, Liu L, Wei X, Zeng S. Toll-Like Receptor 4 (TLR4)/Opioid Receptor Pathway Crosstalk and Impact on Opioid Analgesia, Immune Function, and Gastrointestinal Motility. *Front Immunol*. 2020;11:1455. doi:10.3389/fimmu.2020.01455
19. Costa MJF, de Araujo IDT, da Rocha Alves L, et al. Relationship of Porphyromonas gingivalis and Alzheimer's disease: a systematic review of pre-clinical studies. *Clin Oral Investig*. 2021;25(3):797. doi:10.1007/s00784-020-03764-w
20. Danila D, Partha R, Elrod DB, Lackey M, Casscells SW, Conyers JL. Antibody-labeled liposomes for CT imaging of atherosclerotic plaques: in vitro investigation of an anti-ICAM antibody-labeled liposome containing iohexol for molecular imaging of atherosclerotic plaques via computed tomography. *Tex Heart Inst J*. 2009;36(5):393.
21. Li P, Jin L, Feng L, Wang Y, Yang R. ICAM-1-carrying targeted nano contrast agent for evaluating inflammatory injury in rabbits with atherosclerosis. *Sci Rep*. 2021;11(1):16508. doi:10.1038/s41598-021-96042-y
22. Qi CM, Du L, Wu WH, et al. Detection of Vulnerable Atherosclerotic Plaques in Experimental Atherosclerosis with the USPIO-Enhanced MRI. *Cell Biochem Biophys*. 2015;73(2):331. doi:10.1007/s12013-015-0591-y
23. Gong L, Lei Y, Liu Y, et al. Vaccarin prevents ox-LDL-induced HUVEC EndMT, inflammation and apoptosis by suppressing ROS/p38 MAPK signaling. *Am J Transl Res*. 2019;11(4):2140.
24. Jiang X, Ma C, Gao Y, et al. Tongxinluo attenuates atherosclerosis by inhibiting ROS/NLRP3/caspase-1-mediated endothelial cell pyroptosis. *J Ethnopharmacol*. 2023;304:116011. doi:10.1016/j.jep.2022.116011
25. Reuter S, Gupta SC, Chaturvedi MM, Aggarwal BB. Oxidative stress, inflammation, and cancer: how are they linked? *Free Radic Biol Med*. 2010;49(11):1603. doi:10.1016/j.freeradbiomed.2010.09.006
26. Gabriel SE, Jaakkimainen L, Bombardier C. Risk for Serious Gastrointestinal Complications Related to Use of Nonsteroidal Anti-inflammatory Drugs. *Ann Intern Med*. 1991;115(10):787. doi:10.7326/0003-4819-115-10-787
27. Andrade RJ, Chalasani N, Bjornsson ES, et al. Drug-induced liver injury. *Nat Rev Dis Primers*. 2019;5(1):58. doi:10.1038/s41572-019-0105-0
28. Obaid E, Wu S, Zhong Y, et al. pH-Responsive hyaluronic acid-enveloped ZIF-8 nanoparticles for anti-atherosclerosis therapy. *Biomater Sci*. 2022;10(17):4837. doi:10.1039/D2BM00603K
29. Shen M, Li H, Yao S, et al. Shear stress and ROS-responsive biomimetic micelles for atherosclerosis via ROS consumption. *Mater Sci Eng C Mater Biol Appl*. 2021;126:112164. doi:10.1016/j.msec.2021.112164
30. Wang J, Shangguan P, Chen X, et al. A one-two punch targeting reactive oxygen species and fibril for rescuing Alzheimer's disease. *Nat Commun*. 2024;15(1):705. doi:10.1038/s41467-024-44737-x
31. Spurlock III CF, Tossberg JT, Matlock BK, Olsen NJ, Aune T. Methotrexate Inhibits NF-κB Activity Via Long Intergenic (Noncoding) RNA–p21 Induction. *Arthritis Rheumatol*. 2014;66(11):2947. doi:10.1002/art.38805
32. Spurlock III CF, Gass HMT, Bryant CJ, Wells BC, Olsen NJ, Aune TM. Methotrexate-mediated inhibition of nuclear factor κB activation by distinct pathways in T cells and fibroblast-like synoviocytes. *Rheumatology (Oxford)*. 2015;54(1):178. doi:10.1093/rheumatology/keu279
33. Wang C, He Y, Tang J, et al. Chondroitin sulfate functionalized nanozymes inhibit the inflammation feedback loop for enhanced atherosclerosis therapy by regulating intercellular crosstalk. *Int J Biol Macromol*. 2024;282:136918. doi:10.1016/j.ijbiomac.2024.136918